Tetranuclear Copper(II) and Nickel(II) Complexes Incorporating a New Imidazole-Containing Ligand

Soumen Mukherjee,[a] Thomas Weyhermüller,[a] Eckhard Bill,[a] and Phalguni Chaudhuri*[a]

Keywords: Tetranuclear complexes / Imidazolate bridging / Copper / Nickel / Magnetic properties

The ligating properties of a new tridentate imidazole- and phenol-containing ligand H_3L towards nickel(II) and copper(II) ions have been studied. The ligand generates, in the presence of air and base, iminosemiquinone radical anions, which are not stable in the presence of the metal ions. The amine bond >C–NH– of the parent ligand becomes oxidized to >C=N– bonds upon coordination with Ni^{II} or Cu^{II}. The imidazole N atom becomes deprotonated and the resulting imidazolate group acts as a bridging ligand to generate tetranuclear complexes $[Cu^{II}{}_4L'_4]$ and $[Ni^{II}{}_4L'_4]$, where $[L']^{2-}$ is the dianionic new Schiff base formed after oxidation of the parent ligand. The square-planar tetranickel(II) complex is diamagnetic, as expected, whereas the four copper centres bridged by imidazolate anions in the complex $[Cu^{II}{}_4L'_4]$ are antiferromagnetically exchange coupled (J = –49 cm^{-1}), which has been supported by the EPR measurements. A simple magnetostructural correlation for the imidazolate-bridged copper(II) complexes is yet to emerge.

Introduction

Imidazole (ImH) occurs in proteins as part of the side chain of the amino acid histidine and constitutes all or part of the binding sites of various transition metal ions such as Ni^{2+}, Cu^{2+} or Zn^{2+} in a large number of metalloproteins.[1–4] Particularly, copper–imidazole interactions are widely known in biological systems. As for example, the conjugate base imidazolate ion (Im^-) is present as a bridging ligand between copper(II) and zinc(II) in superoxide dismutase,[5] which catalyses the disproportionation of the harmful superoxide radical anion.

In order to understand the unusual spectroscopic properties and the catalytic mechanisms of copper proteins, the development of relatively simple synthetic models of the active sites of copper proteins is of considerable interest. Since imidazole is present in many natural enzymes and proteins, we have been interested for some time in low molecular weight copper complexes with imidazole[6,7] and imidazolate-containing ligands which may serve as structural as well as spectroscopic models for the active site of copper proteins. As a continuation of this program, we report here a new tridentate ligand, 2,4-di-*tert*-butyl-6-[(5-methyl-3*H*-imidazol-4-ylmethyl)amino]phenol (H_3L) and its copper(II) and nickel(II) complexes.

This new ligand affords tetranuclear complexes, $[L'_4Ni^{II}_4]$ (**1**) and $[L'_4Cu^{II}_4(THF)_4]$ (**2**), where $[L']^{2-}$ is the dianionic Schiff-base form of the parent ligand H_3L after oxidation.

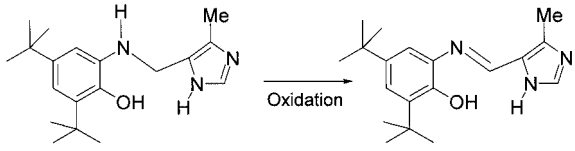

H_3L H_2L'

Complexes **1** and **2** have been characterised not only structurally but also by magnetic susceptibility measurements and EPR spectroscopy, in order to identify the exchange coupling for this tetracopper(II) complex **2** and hopefully to add a new brick to the construction of the correlation between structure and exchange coupling in imidazolate-bridged copper(II) complexes.

Results and Discussion

The ligand H_3L has been prepared in a two-step process involving first a Schiff-base condensation of 6-amino-2,4-di-*tert*-butylphenol with the appropriate 5-methyl-3*H*-imidazole-4-carbaldehyde and the subsequent reduction of the Schiff base by $NaBH_4$ in methanol. The ligand H_3L precipitates as a white solid in an aqueous medium. The ligand was fully characterised by ^1H, ^{13}C NMR, and IR spectroscopy, mass spectrometry and microanalysis together with its melting point determination (see Exp. Sect.). The IR bands due to ν(OH), ν(NH), ν(C–H of *tert*-butyl), ν(C=N), ν(C=C) and ν(C–O) are readily identified for the free H_3L which occur as strong peaks at ca. 3500, 3299, 2959, 1615, 1591 and 1233 cm^{-1}, respectively, and serve as a useful indication for complex formation. There is a distinct

[a] Max Planck Institute for Bioinorganic Chemistry, Stiftstraße 34–36, 45470 Mülheim an der Ruhr, E-mail: chaudh@mpi-muelheim.mpg.de

bathochromic shift typical for coordination of the deprotonated ligand to transition metal centres. The EI mass spectrometric molecular peak at m/z = 315 for H_3L is consistent with the elemental analysis.

A methanolic solution of the ligand, made basic by a few drops of triethylamine, is susceptible to aerial oxidation and forms a radical, presumably an iminosemiquinone, as evidenced by the EPR spectrum (Figure 1) at ambient temperature. A simulation of the spectrum yields the hyperfine coupling constants for the nitrogen atom and three protons to be a_N = 4.74 G, $a_{H(1)}$ = 9.30 G and $a_{H(2)}$ = 3.59 G. The simulated g value of 2.0049 clearly shows that the ligand is "noninnocent" and forms radicals in air. This ligand radical is not stable in the presence of a metal centre, which is shown by the X-ray crystal structures of **1** and **2**, confirming the ligand to be present in an iminophenolate form after complexation. The imine >C=N− character of the coordinated ligand $[L']^{2-}$ is also exhibited in the solid-state IR spectra for **1** and **2**; a sharp strong band appears at 1600 cm^{-1} for **1** and 1595cm^{-1} for **2**.

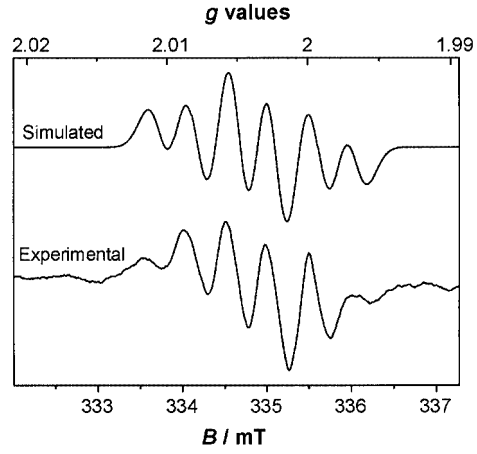

Figure 1. EPR spectrum of the ligand H_3L at room temperature in the presence of triethylamine in methanol

Mass spectrometry in the ESI positive mode (in CH_2Cl_2) is not very helpful in identifying the nuclearity of the nickel(II) complex **1**. The peak at m/z (%) = 683.4 (100) corresponds to the mononuclear species NiL'_2. But for **2**, the Cu^{II} complex, peaks at m/z = 374, 748, 1124 and 1496 with respective isotope distribution clearly show the tetranuclear nature of the copper complex.

Complex **1**, a tetrameric square-planar nickel(II) complex, is diamagnetic as expected, as is evidenced from the magnetic susceptibility as well as the ^1H NMR spectrum. In the ^1H NMR spectrum, the ratio of protons *tert*-butyl/*tert*-butyl/methyl/imine/aromatic/imidazole is 9:9:3:1:2:1, which is to be expected from the oxidized deprotonated ligand (see Exp. Sect.).

Molecular Structure of $[L'_4Ni_4]\cdot 9CH_2Cl_2$ (1)

From a dichloromethane/methanol (1:1) solvent mixture orange red X-ray quality crystals of **1** were obtained and they were subjected to diffractometric studies. The molecule consists of a neutral tetranuclear nickel complex along with 9 CH_2Cl_2 solvent molecules. The neutral molecule with its atom-labelling scheme is shown in Figure 2. Selected bond lengths and angles are listed in Table 1. Each of the nickel centres is in a distorted square-planar geometry with N_2O coordination from the deprotonated ligand and the fourth donor atom being the nitrogen atom of the imidazolate ring originating from the adjacent NiN_2O unit. Worth noting is the short C(8)−N(7) distance of 1.297(11) Å with a >C=N− character indicating oxidation of the >CH_2−NH− bond of the ancillary ligand H_3L. The average Ni−O (phenol), Ni−N (imine), Ni−N (imidazole) and Ni−N (adjacent imidazole) bond lengths of 1.856, 1.850, 1.891 and 1.850 Å, respectively, are similar to those in other square-planar Ni^{II} complexes.[8] The four nickel centres are arranged in the form of a "butterfly" with the Ni(1)−Ni(1A)−Ni(1B) and Ni(1C)−Ni(1A)−Ni(1B) planes forming the "wings" of the butterfly (see b in Figure 2).[9] The dihedral angle between these two planes is 107.7°. All the adjacent Ni···Ni distances are equal with a value of 5.851 Å.

Molecular Structure of $[L'_4Cu_4(THF)_4]$ (2)

Although the analytical data unambiguously show the presence of a CuL′ core as the smallest unit in **2**, the magnetic susceptibility data exhibit a strong temperature dependence with effective moments as 1.52 μ_B at 290 K and 0.09 μB at 2 K, refuting the mononuclear formulation. Hence, an X-ray analysis was undertaken to remove the doubts regarding connectivity. Unfortunately, crystals of **2** obtained from a THF/methanol mixture diffract X-rays very weakly.[10] In spite of the high R factor and large standard deviations due to the severity of the disorder and weakness of the data collected from a poorly diffracting small crystal, the crystal structure analysis of **2** confirmed its tetranuclear nature. Because of its unacceptable quality, we are unable to publish the crystal data in detail. It is not clear how many THF molecules are present in the unit cell. The structure consists of distinct $[L'_4Cu_4(THF)_4]$ molecules (Figure 3).

Selected interatomic distances and angles are given in Table 2. As observed in **1**, oxidation of the ligand occurs at the same position [C(8)−N(7) = 1.31 Å]. The structure consists of a distorted square-pyramidal tetranuclear neutral molecule with the Cu centres forming a "butterfly structure" (Figure 3). A THF molecule occupies the fifth position of the coordination site in each copper centre. The dihedral angle between the plane defined by connecting Cu(1)−Cu(2)−Cu(4) and Cu(3)−Cu(2)−Cu(4) is 150.1°. The average Cu−O (phenol), Cu−N (imine), Cu−N (imidazolate) and Cu−N (imidazolate of adjacent ligand) bond lengths are 1.942 Å, 1.942 Å, 1.992 Å and 1.948 Å, respectively, which are similar to other square-planar/pyramidal Cu^{II} complexes.[6,7,11] It is observed that the Cu(1)−N(10) bond is more elongated than it is for the other coordinating atoms. This tendency is the same for the other copper centres and is due to a Jahn−Teller effect which is present for d^9 systems thus making **2** less symmetric than **1**, a d^8

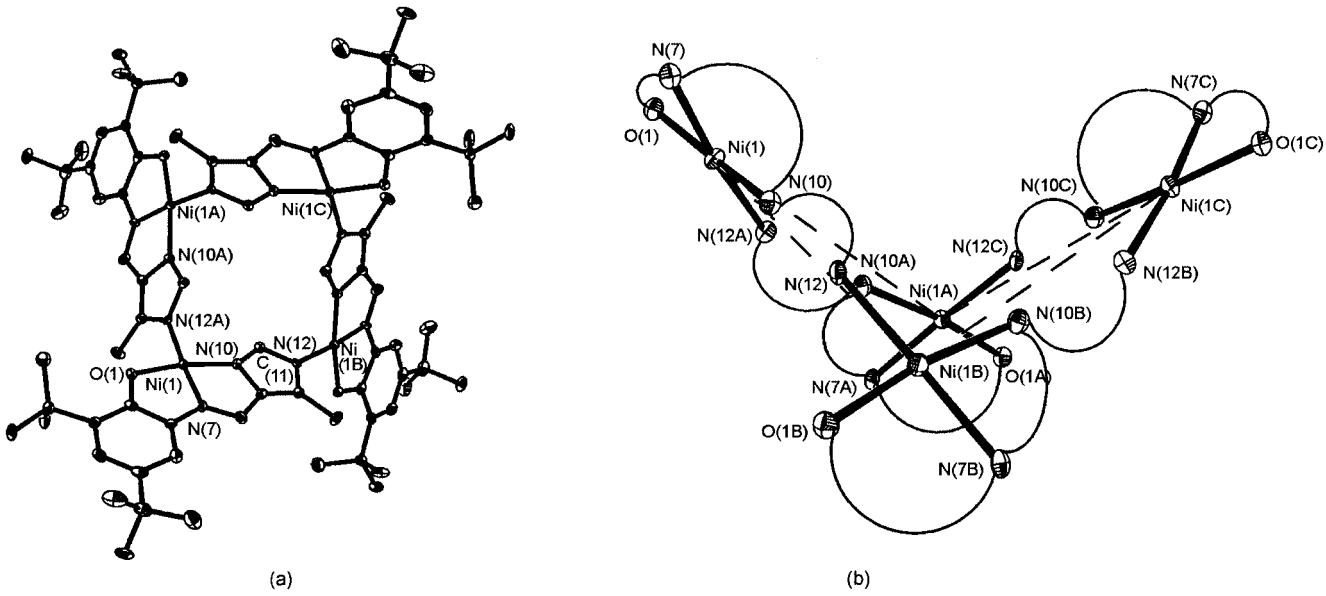

Figure 2.(a) ORTEP diagram of $[Ni_4L'_4]$ **1**; (b) view of **1** highlighting the butterfly nature of the four nickel centres; the ligand is denoted only by the donor atoms joined by the curved lines

Table 1. Selected bond lengths [Å] and angles [°] for **1**

Ni(1)−N(7)	1.850(7)	C(4)−C(5)	1.405(12)
Ni(1)−N(12A)	1.891(6)	C(5)−C(6)	1.405(11)
Ni(1)−N(10)	1.885(7)	C(1)−C(6)	1.407(12)
Ni(1)−O(1)	1.856(5)	C(9)−N(10)	1.381(10)
C(1)−O(1)	1.355(9)	N(12)−C(11)	1.332(11)
C(6)−N(7)	1.391(10)	C(13)−N(12)	1.362(10)
N(7)−C(8)	1.297(11)	C(11)−N(10)	1.297(11)
C(1)−C(2)	1.396(11)	C(8)−C(9)	1.447(11)
C(2)−C(3)	1.411(12)	C(9)−C(13)	1.370(11)
C(3)−C(4)	1.368(13)	C(13)−C(14)	1.489(11)
Ni(1A)−Ni(1)−Ni(1B)	77.8		
O(1)−Ni(1)−N(7)	86.5(3)	N(12A)−Ni(1)−N(10)	94.1(3)
N(7)−Ni(1)−N(10)	84.0(3)	N(12A)−Ni(1)−O(1)	95.6(3)
N(7)−Ni(1)−N(12A)	174.6(3)	N(10)−Ni(1)−O(1)	170.2(3)
C(1)−O(1)−Ni(1)	111.8(5)	Ni(1)−N(10)−C(9)	112.4(5)
C(8)−N(7)−C(6)	129.8(7)	C(11)−N(12A)−Ni(1)	123.8(5)
Ni(1)−N(10)−C(11)	142.8(6)	C(13)−N(12A)−Ni(1)	130.5(5)
C(8)−N(7)−Ni(1)	117.3(6)	C(6)−N(7)−Ni(1)	112.8(5)
Ni(1)···Ni(1A)	5.851		
Ni(1A)···Ni(1B)	7.351		

system; Cu(1) is displaced by 0.11 Å from the mean basal plane of the three nitrogen atoms [N(7), N(10), N(42)] and one oxygen atom [O(1)]. The dihedral angles between the plane N(42)O(1)N(7)N(10) containing the Cu(1) ion and the planes N(42)C(43)C(39)N(40)C(41) and N(10)-C(9)C(13)N(12)C(11) describing the two imidazolate bridging groups are 47.2° and 82.2°, respectively. It is interesting to note that the angle between the Cu(1)−N_{im}(42) and Cu(2)−N_{im}(40) vectors is 142.2° and that between the Cu(1)−N_{im}(10) and Cu(4)−N_{im}(12) vectors is 132.6°. The angle between the planes defined by Cu(1)O(1)N(7)N-(10)N(42) and Cu(2)O(31)N(37)N(40)N(72) is 139.1°.

Magnetochemistry and EPR Studies with 2

The magnetic susceptibility data for a polycrystalline sample of **2** was measured from 2 to 290 K in an applied magnetic field of 1 T to characterise the nature and magnitude of the exchange interaction propagated by the bridging ligands. The Heisenberg spin Hamiltonian used was in the form $\hat{H} = -2J \sum_{ij} \vec{S}_i \cdot \vec{S}_j$ for an isotropic exchange coupling. The experimental magnetic data were simulated using a least-squares fitting computer program[12] with a full-matrix diagonalisation of exchange coupling, Zeeman splitting,

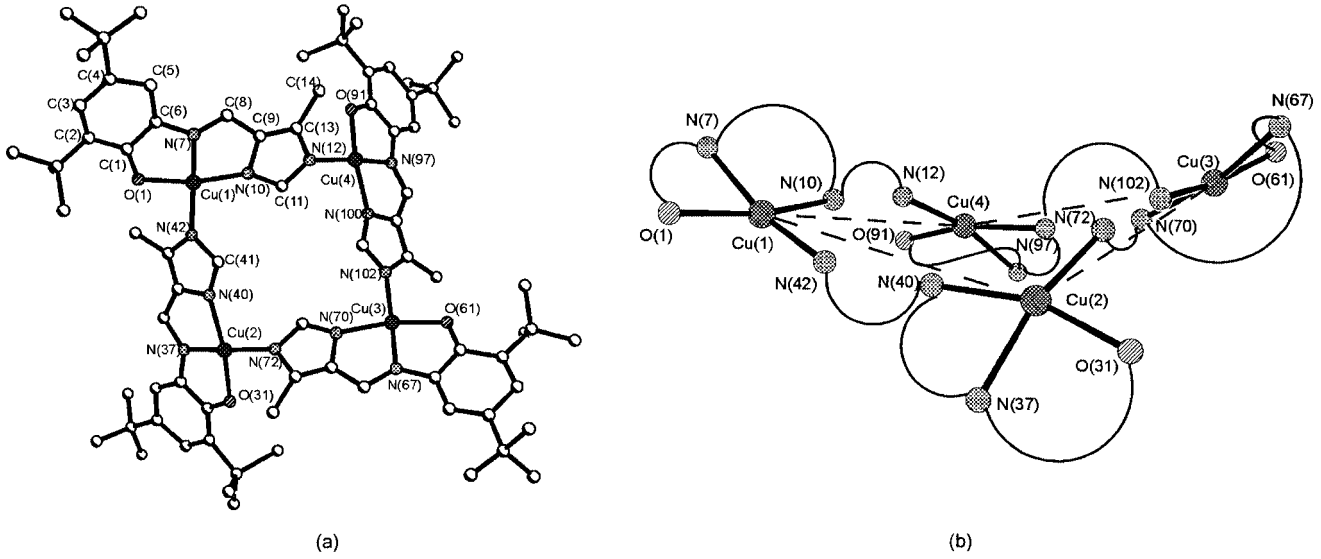

Figure 3.(a) Molecular structure of $[Cu_4L'_4]$ **2**; (b) view of **2** highlighting the butterfly dispositions of the copper centres

Table 2. Selected bond lengths [Å] and angles [°] for **2**

Cu(1)−N(7)	1.913(17)	Cu(2)−N(37)	1.964(16)
Cu(1)−N(42)	1.925(17)	Cu(2)−N(72)	1.957(16)
Cu(1)−N(10)	1.952(16)	Cu(2)−N(40)	2.020(16)
Cu(1)−O(1)	1.955(12)	Cu(2)−O(31)	1.965(13)
C(1)−O(1)	1.316(25)	C(9)−N(10)	1.462
C(6)−N(7)	1.420	N(12)−C(11)	1.347
N(7)−C(8)	1.310	C(13)−N(12)	1.408
C(1)−C(2)	1.422	C(11)−N(10)	1.381
C(2)−C(3)	1.399	C(8)−C(9)	1.461
C(3)−C(4)	1.365	C(9)−C(13)	1.341
C(4)−C(5)	1.399	C(13)−C(14)	1.525
C(5)−C(6)	1.409		
C(1)−C(6)	1.377		
Cu(1)−Cu(2)−Cu(3)	89.8	Cu(3)−Cu(4)−Cu(1)	89.8
Cu(2)−Cu(3)−Cu(4)	86.3	Cu(4)−Cu(1)−Cu(2)	85.9
O(1)−Cu(1)−N(7)	82.6	O(31)−Cu(2)−N(37)	81.6
N(7)−Cu(1)−N(10)	83.4	N(37)−Cu(2)−N(40)	81.7
N(7)−Cu(1)−N(42)	164.7	N(37)−Cu(2)−N(72)	163.2
N(42)−Cu(1)−N(10)	99.5	N(72)−Cu(2)−O(31)	93.8
N(42)−Cu(1)−O(1)	94.2	N(72)−Cu(2)−N(40)	100.9
N(10)−Cu(1)−O(1)	166.0	N(40)−Cu(2)−N(31)	162.7
Cu(1)−N(10)−C(11)	146.14(16)	Cu(2)−N(40)−C(41)	142.8(17)
Cu(1)−N(42)−C(41)	123.59(16)	Cu(4)−N(12)−C(11)	123.89(16)
Cu(1)···Cu(2)	6.054	Cu(3)···Cu(4)	6.034
Cu(1)···Cu(4)	6.044	Cu(1)···Cu(3)	8.524
Cu(2)···Cu(3)	6.019	Cu(2)···Cu(4)	8.245

and axial single-ion zero-field interactions $D\vec{S}_z^{\,2}$, if necessary. The susceptibility data were corrected for diamagnetism (Pascal corrections), temperature-independent paramagnetism (TIP) and the presence of paramagnetic monomer impurities (P) in the following way: $\chi_{calcd.} = (1 - P)\chi + \chi_{TIP} + P\chi_{mono}$.

The nature of the μ_{eff} vs. T plot for **2** (Figure 4) shows a behaviour typical for antiferromagnetic spin coupling. The effective moment μ_{eff} decreases monotonically with the decrease in temperature; the values of μ_{eff} are 3.051 μ_B at 290 K and 0.180 μ_B at 2 K. The magnetic data reveal an energetically well-isolated ground state of total spin $S_t = 0$, discernible from the decline of effective moments at temperatures below 100 K. The residual moment of 0.180 μ_B at 2 K is attributed to a monomeric ($S = 1/2$) impurity (2.0%). Monomeric species were also detected in weak abundance in the EPR spectra, as will be mentioned later. The susceptibility data could be simulated considering exchange coupling between adjacent Cu^{II} pairs with local spins ($S = 1/2$), as shown in the inset in Figure 4. The multiplets $|S_A S_B S_t>$ are labelled by the "pair spins", S_A ($\vec{S}_A = \vec{S}_1 + \vec{S}_3$) and S_B ($\vec{S}_B = \vec{S}_2 + \vec{S}_4$). The ground state is a singlet $|S_A S_B S_t> = |110>$ and the first excited state at energy $2J$ is a triplet $|111>$ (Figure 4). The states $|011>$, $|000>$ and $|101>$ are degenerate at energy $4J$ and the highest state at energy $6J$ is a quintuplet $|112>$. In zero field the multiplets remain degenerate in energy with pure magnetic quantum numbers,

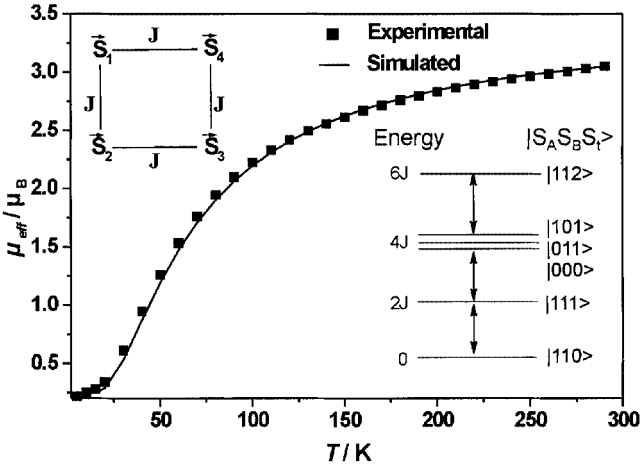

Figure 4. Plot of μ_{eff} vs. T for **2**; the solid line represents the simulated curve; insets: model used to simulate the spin coupling in **2** and corresponding spin states resulting from the spin Hamiltonian used (see text)

according to their multiplicity. Projections of local spins S_i on the total spin S_t ($\vec{S}_t = \vec{S}_A + \vec{S}_B$)[13] reveal identical g_t values for all multiplets $S_t \neq 0$. The simulation of the experimental susceptibility data for the tetramer yielded an exchange coupling constant $J = -49$ cm^{-1}, $g = 2.022$, a paramagnetic impurity (P: $S = {}^1/_2$) of 2% and a temperature-independent paramagnetism (TIP) of 240×10^{-3} emu.

X-band EPR spectra for **2** in the solid state from 11.7 K to 62.1 K are dominated by a strong almost isotropic signal at $g = 2.08$ which shows the usual Curie behaviour, $I \sim 1/T$, for the given temperature range. Therefore, the strong derivative signal at $g \approx 2$ is attributed to the monomeric paramagnetic impurity (2%) present in the solid-state susceptibility measurements. In addition to the prominent line there are a number of weak signals in the measured field range extending from 50 to 600 mT. Their appearance is typical of integer spin manifolds arising for the exchange-coupled Cu^{II} tetramer, because competing Zeeman and zero-field splitting are expected due to dipolar coupling and anisotropic exchange. As a consequence, the resonances are widely spread over a large field range and the derivative signals appear to be weak (not the intensity). On increasing the temperature, changes in the relative intensities of these features are observed between 150 and 260 mT and between 380 and 600 mT (Figure 5), which is typical of integer spin signals from excited spin multiplets.

In order to elucidate the correlation between the EPR spectra and the spin multiplets of the coupled system, the change of intensity (I) of the derivative peak at 480 mT was scanned over the entire temperature (T) range. As the population of the excited state in the first order is dependent on the Boltzmann function of resonating levels, the product intensity·temperature, $I \cdot T$, was plotted versus temperature (Figure 5b). The fading below 10 K and the strong rise at elevated temperatures prove that the signals arise from excited states and that the ground state is diamagnetic and EPR-silent, in accordance with the susceptibility findings. For quantitative analysis, the experimental data were compared with the theoretical Boltzmann functions derived from the spin-coupling model (Figure 4). It is to be noted that values up to 40 K were taken as line broadening, which occurs above this temperature. The best agreement was obtained for $I_{111}T$, describing the thermal population of the first excited triplet state $|111>$, $I_{111}\ T \approx [\exp(2J/kT)]/Z$, where $Z = 1 + 3\exp(2J/kT) + 7\exp(6J/kT) + 5\exp(12J/kT)$. The solid line is a fit with $J = -42$ cm^{-1}, which is close to the exchange coupling constant of $J = -49$ cm^{-1} evaluated from the susceptibility measurements. Therefore, particular non-Kramers resonance at $B = 480$ mT, and probably the whole complex EPR spectrum in the field range 380−600 mT appears to arise from the first excited triplet state $|111>$ of the tetramer.

In an imidazolate-bridged system, there can be two pathways used to explain the magnetic interaction, viz. the σ- and the π-exchange pathways. Generally, it is agreed that the π orbitals are not involved in the coupling.[7,14] It has been stated that, since the magnetic orbitals are σ-antibonding for square-planar and square-pyramidal complexes, the relevant exchange pathway through the imidazolate bridge is of the σ-type. The imidazolate orbitals responsible for this sort of interaction are essentially parallel to the N−N′ (or C−C) direction.[7,11c]

Several studies have already been reported,[7,11c] in which structural data have been used to find correlations between structure and exchange coupling in imidazolate-bridged copper(II) complexes. Comparison of the numerical data shows that a simple magnetostructural correlation for imidazolate-bridged Cu complexes does not exist. However, as the values of J are independent of θ, the angle between the copper and imidazole coordination planes, a π-exchange pathway can be discarded. It has been concluded from EHMO calculations[11c] that the extent of anti-ferromagnetic coupling will increase when the N−N and other Cu−N bonds are parallel to the imidazolate carbon−carbon bond, thus favoring a σ-exchange pathway. Although the coupling constant for **2** is strong compared with the other complexes, the values of J cannot be strictly attributed to the values of α, the angle between the Cu−N and N−N vectors. This indicates that σ-superexchange cannot be the only mechanism for the exchange coupling for

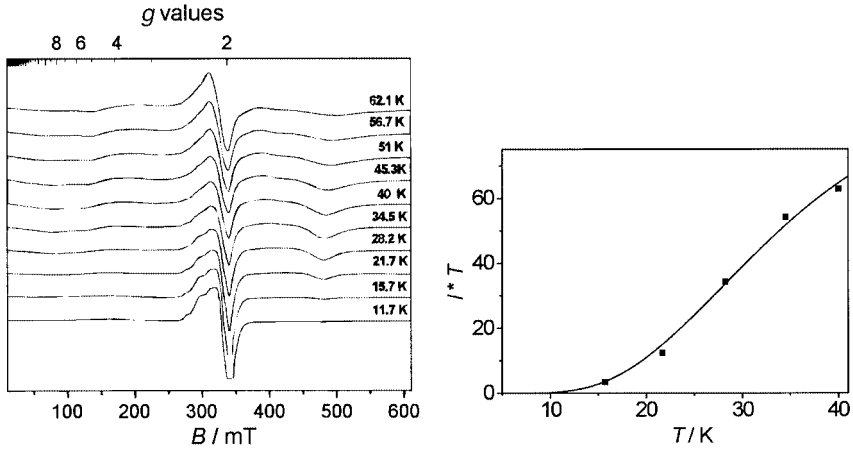

Figure 5. (a) EPR spectra of a powdered sample of **2** recorded as a function of temperature; (b) temperature dependence of the temperature-weighted intensity ($I \cdot T$) of the EPR subspectra; the solid line is the calculated Boltzmann function $I_{111} \cdot T$ with $J = -42$ cm^{-1}

this compound. The presence of ligand−ligand interactions may also play a part in this type of exchange coupling. Recently, a theoretical DFT study[15] on the magneto-structural correlation in imidazolate-bridged dicopper(II) complexes showed that the exchange coupling constant *J* mainly depends on the Cu−*N*−C(Im) bond angle and is insensitive to the variation of the Cu−N(Im) distance and the dihedral angle between the bridged imidazolate ring and copper coordination planes.

Concluding Remarks

The ligating properties of a new tridentate ligand, 2,4-di-*tert*-butyl-6-[(5-methyl-3*H*-imidazol-4-ylmethyl)amino]-phenol containing an imidazole N-donor atom together with a phenol O-donor and amine N-donors towards the nickel(II) and copper(II) centers are described. The imidazole N atom becomes deprotonated and the resulting imidazolate group serves as a bridging ligand to generate tetranuclear complexes of the said metal centres. Although the ligand generates the iminosemiquinone monoanion radical very easily in the presence of a base and air, as evidenced by EPR spectroscopy, the radical form could not be stabilized in the presence of the metal centres. The C−NH bonds from the parent ligand have been oxidized to C=N bonds upon coordination with the Ni^{II} or Cu^{II} centres. The realization that the present phenol as well as imidazole-containing ligand can generate polynuclear complexes highlights the prospect of designing a generic ligand system, which should form polynuclear species with other metal centres.

The imidazolate-bridged copper(II) complexes are, as expected, antiferromagnetically exchange-coupled yielding diamagnetic ground states. No simple magneto-structural correlation has yet emerged for these imidazolate-bridged complexes. The synthesis of more of these imidazolate-bridged copper(II) complexes would therefore be warranted in order to resolve this complex problem of magnetostructural correlation.

Experimental Section

Materials and Physical Measurements: Commercial grade chemicals were used for synthetic purposes, and solvents were distilled and dried before use. Fourier transform IR spectroscopy on KBr pellets was performed with a Perkin−Elmer 2000 FT-IR instrument. Mass spectra were recorded either in the EI or the ESI (in CH_2Cl_2) modes with a Finnigan MAT95 or 8200 spectrometer. Magnetic susceptibilities of the polycrystalline samples were recorded with a SQUID magnetometer (MPMS, Quantum Design) in the 2−290 K temperature range with an applied field of 1 T. Diamagnetic contributions were estimated for each compound by the use of Pascal's constants. ^1H and ^{13}C NMR spectra were recorded using a Bruker ARX 250, or DRX 400 spectrometer. The spectra are referenced to TMS, using the ^{13}C or residual ^1H signals of the deuterated solvents as internal standards. X-band EPR spectra were recorded with a Bruker ESP 300E spectrometer equipped with a helium flow cryostat (Oxford Instruments ESR 910), an NMR field probe (Bruker 035M) and a microwave frequency counter HP 5352B.

X-ray Crystallographic Data Collection and Refinement of the Structures: A single crystal of **1** was coated with perfluoropolyether, picked up with glass fibres, and mounted on a Nonius Kappa-CCD diffractometer equipped with a cryogenic nitrogen cold stream operating at 100(2) K. Graphite-monochromated Mo-K_α radiation (λ = 0.71073 Å) was used. Intensity data were corrected for Lorentz and polarisation effects. The intensity data set of **1** was corrected for absorption with the program SADABS[16] The Siemens SHELXTL software package[17] was used for solution, refinement, and artwork of the structure, and neutral atom scattering factors of the program were used. All structures were solved and refined by direct methods and difference Fourier techniques. Non-hydrogen atoms were refined anisotropically, and hydrogen atoms were placed at calculated positions and refined as riding atoms with isotropic displacement parameters. Details of data collection and structure refinements are summarized in Table 3. CCDC-236872 contains the supplementary crystallographic data for this paper. These data can be obtained free of charge at www.ccdc.cam.ac.uk/conts/retrieving.html [or from the Cambridge Crystallographic Data Centre, 12 Union Road, Cambridge CB2 1EZ, UK; Fax: + 44-1223-336-033; E-mail: deposit@ccdc.cam.ac.uk].

Table 3. Crystal data and structure refinement for **1**, $[Ni_4L'_4]\cdot 9CH_2Cl_2$

	1
Empirical formula	$C_{76}H_{100}N_{12}Ni_4O_4\cdot 9CH_2Cl_2$
Formula mass	2244.85
Temperature [K]	100(2)
Wavelength [Å]	0.71073
Crystal system	tetragonal
Space group	$P\bar{4}2_1/c$ (No. 114)
Unit cell dimensions [Å]	a = 20.74(3)
	c = 12.1538(10)
Volume [Å^3]; Z	5227.9(12); 2
Density (calcd.) [Mg/m^3]	1.426
Absorp. coeff. [mm^{-1}]	1.220
F(000)	2324
θ range for data collection [°]	1.94−25.00
Index ranges	$-31 \le h \le 32$
	$-10 \le k \le 31$
	$-18 \le l \le 17$
Reflections collected	39793
Independent reflections	4608
Absorption correction	SADABS
Data/restraints/parameters	4591/16/289
Goodness-of-fit on F^2	1.048
Final R int [$I > 2\sigma(I)$]	$R1$ = 0.0786, $wR2$ = 0.2180
R int (all data)	$R1$ = 0.0982, $wR2$ = 0.2366

Ligand Synthesis

2,4-Di-*tert*-butyl-6-[(5-methyl-3*H*-imidazol-4-ylmethyl)amino]-phenol (H_3L): 2-Amino-4,6-di-*tert*-butylphenol (2.2 g, 10 mmol) and 5-methyl-3*H*-imidazole-4-carbaldehyde (1.1 g, 10 mmol) were added to deaerated methanol (50 mL) and the resulting solution was refluxed under argon for 2 h. The red solution was cooled and $NaBH_4$ was added portionwise until the solution turned a faint yellow. The precipitation of a white solid was initiated by dropwise addition of water. The white solid was collected by filtration and dried under vacuum. Yield: 2.8 g (89%). M.p. 186 °C. $C_{19}H_{29}N_3O$ (315.5): calcd. C 72.34, H 9.27, N 12.84; found C 71.0, H 9.2, N

12.8. ^{1}H NMR ([D$_6$]DMSO): δ = 1.21 (s, 9 H), 1.31 (s, 9 H), 2.15 (s, 3 H), 4.02 (s, 2 H), 6.5 (t, 2 H), 7.4 (s, 1 H) ppm. ^{13}C NMR ([D$_6$]DMSO): δ = 30.0 (s), 34.1 (s), 34.5 (s), 48.6 (s), 107.5 (s), 111.1 (s), 133.2 (s), 136.3 (s), 140.3 (s), 141.9 (s) ppm. IR (KBr): $\tilde{\nu}$ = 3299 s, 2959 s, 1615 s, 1591 s, 1233 s cm^{-1}. EI-MS: *m*/*z* = 315 [M$^+$].

Complex 1 [Ni$_4$L′$_4$]: The ligand H_3L (1 mmol, 0.315 g) was dissolved in 25 mL of deaerated methanol. Solid $Ni(ClO_4)_2 \cdot 6H_2O$ (1 mmol, 0.365 g) along with NEt_3 (0.15 mL) were added to the ligand solution. The resulting orange-red solution was refluxed under argon for 1 h and then stirred in air for 0.5 h, whereupon a microcrystalline orange-red solid precipitated. The solid was filtered, dried in air. Yield: 0.21 g (58%). $C_{76}H_{100}N_{12}Ni_4O_4$ (1480.5): calcd. C 61.66, H 6.81, N 11.35, Ni 1586; found C 58.8, H 5.8, N 10.7, Ni 15.5. IR (KBr): $\tilde{\nu}$ = 2952, 1600, 1474, 1399, 1253, 1130, 861 cm^{-1}. X-ray quality crystals for **1** $[Ni_4L_4] \cdot 9CH_2Cl_2$ were obtained from a mixture of dichloromethane/methanol (1:1).

Complex 2 [Cu$_4$L′$_4$]: The ligand H_3L was dissolved in 15 mL of methanol. Solid $Cu(CH_3COO)_2 \cdot 4H_2O$ (0.5 mmol, 0.10 g) was added to the ligand solution, and the whole solution was made basic by adding NEt_3 (0.15 mL). The resulting light orange-red solution was refluxed for 1 h and then cooled to room temperature, whereupon a red-orange microcrystalline solid precipitated. The microcrystalline solid separated by filtration was recrystallised from a tetrahydrofuran/methanol solvent mixture. Yield: 0.120 g (64%). $C_{76}H_{100}Cu_4N_{12}O_4$ (1499.9): calcd. C 60.86, H 6.72, Cu 16.95, N 11.21; found C 59.8, H 6.6, Cu 17.3, N 11.1. IR (KBr): $\tilde{\nu}$ = 2951, 1595, 1470, 1398, 1257, 1126, 857, 647 cm^{-1}.

Acknowledgments

Financial support from the DFG (Priority Program Ch111/2-2) is gratefully acknowledged. Thanks go to Mrs. H. Schucht and Mr. A. Göbels for skilful technical assistance.

[1] T. E. Creighton, in *Proteins, Structures and Molecular Properties* (Ed.: W. H. Freeman), New York, **1984**.
[2] H. C. Freeman, in *Inorganic Biochemistry* (Ed.: G. L. Eichhorn), Elsevier, New York **1973**, chapter 4.
[3] R. J. Sundberg, R. B. Martin, *Chem. Rev.* **1974**, *74*, 471.
[4] "Bioinorganic Chemistry − State of the Art", *J. Chem. Educ.* **1985**, *62*, 917−1001.
[5] J. S. Richardson, K. A. Thomas, B. H. Rubin, D. C. Richardson, *Proc. Natl. Acad. Sci. U. S. A.* **1975**, *72*, 1349.
[6] P. Chaudhuri, I. Karpenstein, M. Winter, C. Butzlaff, E. Bill, A. X. Trautwein, U. Flörke, H.-J. Haupt, *J. Chem. Soc., Chem. Commun.* **1992**, 321.
[7] P. Chaudhuri, I. Karpenstein, M. Winter, M. Lengen, C. Butzlaff, E. Bill, A. X. Trautwein, U. Flörke, H.-J. Haupt, *Inorg. Chem.* **1993**, *32*, 888 and references cited therein.
[8] For example: D. J. White, N. Laing, H. Miller, S. Parsons, S. Coles, P. A. Tasker, *Chem. Commun.* **1999**, 2077.
[9] V. V. Pavlishchuk, S. V. Kolotilov, A. W. Addison, M. J. Prushan, D. Schollmeyer, L. K. Thomspon, E. A. Goreshnik, *Angew. Chem. Int. Ed.* **2001**, *40*, 4734.
[10] $[C_{76}H_{100}N_{12}Cu_4\ (C_4H_8O)_4] \cdot x$THF, monoclinic, space group $P2_1/c$, a = 24.916(5) Å, b = 17.296(4) Å, c = 33.004(7) Å, β = 91.72°, V = 14216 Å^3, Z = 4, T = 100(2) K, final R = 0.151 for 10569 independent reflections.
[11] Selected references: [11a] G. Ivarsson, B. K. S. Lundberg, N. Ingri, *Acta Chem. Scand.* **1972**, *26*, 3005. [11b] Kolks, S. J. Lippard, J. V. Waszczak, H. R. Lilienthal, *J. Am. Chem. Soc.* **1982**, *104*, 717. [11c] A. Bencini, C. Benelli, D. Gatteschi, C. Zanchini, *Inorg. Chem.* **1986**, *25*, 398. [11d] C. A. Salata, M. T. Youinou, C. J. Burrows, *Inorg. Chem.* **1991**, *30*, 3454. [11e] H. Nie, S. M. J. Aubin, M. S. Mashuta, R. A. Porter, J. F. Richardson, D. N. Hendrickson, R. M. Buchanan, *Inorg. Chem.* **1996**, *35*, 3325. [11f] G. Tabbi, W. L. Driessen, J. Reedijk, R. P. Bonomo, N. Veldman, A. J. Spek, *Inorg. Chem.* **1997**, *36*, 1168. [11g] N. Matsumoto, Y. Motoda, T. Matsuo, T. Nakashima, N. Re, F. Dahan, J.-P. Tuchagues, *Inorg. Chem.* **1999**, *38*, 1165. [11h] E. Colacio, M. Ghazi, R. Kivekäs, M. Klinga, F. Lloret, J. M. Moreno, *Inorg. Chem.* **2000**, *39*, 2770.
[12] V. Staemmler, F. Birkelbach, C. Krebs, unpublished, Bochum, Germany, **1997**.
[13] A. Bencini, D. Gatteschi, *Electron Paramagnetic Resonance of Exchange Coupled Systems*, Springer-Verlag, Berlin **1990**.
[14] [14a] D. N. Hendrickson, M. S. Haddad, *Inorg. Chem.* **1978**, *17*, 2622. [14b] M. S. Haddad, E. N. Duester, D. N. Hendrickson, *Inorg. Chem.* **1979**, *18*, 141. [14c] C. Benelli, R. K. Bunting, D. Gatteschi, C. Zanchini, *Inorg. Chem.* **1984**, *23*, 3074.
[15] Y.-M. Sun, C.-B. Liu, X.-J. Lin, S. W. Bi, *New J. Chem.* **2004**, *28*, 270.
[16] G. M. Sheldrick, University of Göttingen, Germany, **1994**.
[17] G. M. Sheldrick, *SHELXL-97, Program for refinement of crystal structures and program for solution of crystal structures*, University of Göttingen, Germany, **1997**.

Received April 29, 2004
Early View Article
Published Online September 2, 2004

